Protein Denaturation in Nonlinear Isocratic and Gradient Elution Chromatography

Roger D. Whitley, Xiaomang Zhang, and N.-H. Linda Wang
School of Chemical Engineering, Purdue University, West Lafayette, IN 47907

Protein denaturation, common in hydrophobic adsorption systems, causes misinterpretation of adsorption mechanisms, interferes with analysis in analytical chromatography, and complicates the design of large-scale adsorption processes. A detailed adsorption model isolates the effects due to denaturation from those due to mass transfer and intrinsic adsorption kinetics. The model is verified using protein gradient elution data. Simulations establish that typical symptoms of denaturation in frontal and elution chromatograms include sensitivity to changes in feed composition, column length, particle size, and operating conditions (feed size, flow rate, and column history). When a denatured species adsorbs irreversibly, the elution chromatogram shows decreasing peak area with increasing incubation time and apparent adsorption hysteresis over repeated cycles. In gradient elution, the peak elution order, resolution, and relative peak height depend highly on modulator properties and operating conditions. Interfering species limit solid-phase induced denaturation by competing for binding sites. Strategies for detecting and minimizing denaturation are proposed.

Introduction

Chromatography is one of the most important methods for the separation of polypeptides and proteins (Scopes, 1982; Regnier, 1987). However, protein denaturation is a common problem in chromatographic separation, especially in reversed-phase liquid chromatography (RPLC) and hydrophobic interaction chromatography (HIC). Denaturation is essentially due to the significant alteration of a protein's complex structure and properties by changes in factors such as pH, ionic strength, or temperature. The addition of solvents and denaturants (urea, heavy metals) or contact with foreign surfaces can also alter protein conformation. Denaturation can greatly reduce protein recovery and separation in preparative chromatography and may lead to misinterpretation of adsorption mechanisms, errors in parameter estimation, and sample purity analysis. Hence, it is important to investigate why and how protein denaturation occurs and how to detect and minimize denaturation in chromatography (Zhang, 1991). This study will focus on the latter issue.

Protein denaturation in RPLC

The problem of protein denaturation is most severe in RPLC because it uses a nonpolar stationary phase, an organic solvent as eluent and an acidic mobile phase (Regnier, 1987). The fundamental protein structure consists of a hydrophobic interior and a hydrophilic exterior. When a protein contacts the hydrophobic silica surface in RPLC, its inner hydrophobic part will wholly or partially be exposed in order to minimize the total free energy. As a result, the external hydrophobicity of a denatured protein will be quite different from that of a native one (Cohen et al., 1984a,b, 1985; Hearn and Grego, 1984; Hearn and Aguilar, 1987). Investigations of protein adsorption mechanisms have revealed multiple adsorbed states, and depending on protein and conditions, proteins can undergo conformational changes during contact with sorbent surfaces (Benedek et al., 1984; Andrade, 1985; Andrade and Hlady, 1987; Lu et al., 1986, 1988; Lin and Karger 1990). These results are in good agreement with the observation that a hydrophobic

Correspondence concerning this article should be addressed to N.-H. Linda Wang.
Current address of R. D. Whitley: Air Products and Chemicals, Inc., 7201 Hamilton Blvd., Allentown, PA 18195.
Current address of X. Zhang: Dept of Chemical Engineering, University of Wisconsin-Madison, Madison, WI 53706.

stationary surface can catalyzes the unfolding of peptides to make them more hydrophobic (Jacobson et al., 1984). Direct spectral studies (FTIR, fluorescence, photoacoustic, photodiode array) also indicate that when a protein contacts the RPLC sorbent, conformational changes occur in the chromatographic contacting area of the protein (Katzenstein et al., 1986; Lu et al., 1988).

Protein denaturation in other types of chromatography

Protein conformational changes are also found in other types of chromatography, such as HIC (Ingraham et al., 1985; Wetlaufer and Koenghauer, 1986; Wu et al., 1986a,b; Kunitani et al., 1988; Oroszlan et al., 1990), ion-exchange chromatography (Parente et al., 1984a,b), and affinity chromatography (Jaulmes and Vidal-Madjar, 1989).

Although HIC is conducted with weakly hydrophobic surfaces and in general with high concentrations of stabilizing salts (for example, ammonium sulfate), conformational changes can happen, depending on the mobile phase, column temperature, hydrophobicity of the stationary surface, and the protein itself. Several examples of multiple-peak formation have been observed in the hydrophobic interaction mode of protein purification (Ingraham et al., 1985; Wu et al., 1986a,b). Since HIC is inherently less denaturing, reversible tertiary protein denaturation can be mediated through adsorption on HIC column surfaces (Wu et al., 1986a). Quaternary subunit dissociation of tumor necrosis factor (TNF) has been observed on an HIC column, resulting in four peaks from a single homogeneous sample (Kunitani et al., 1988). Jennissen (1987) discusses isotope tracer experiments which indicate that adsorption hysteresis of phosphorylase *b* on butyl-Sepharose may be caused by a combination of conformational reactions and reorientation reactions.

For ion-exchange chromatography, Parente et al. (1984a,b) reported the effects of urea and temperature on the denaturation of lysozyme and α-chymotrypsinogen. Denaturation was evident by a remarkable decrease in capacity factor. The elution profile obtained under partially denaturing conditions showed a strong flow rate dependence because the rate of denaturation was of the same order as convection rate.

Reversible and irreversible denaturation

Some surface-induced protein denaturation is reversible, which means some of the denatured molecules can refold to the native form in solution (Cohen et al., 1985; Kunitani et al., 1988). Thus, reinjection of the denatured peak can result in both native and denatured peaks. For irreversible denaturation processes the denatured form cannot refold to the native form (Cohen et al., 1984a; Benedek et al., 1984; Karger and Blanco, 1989). As column contacting time increases, the denatured form increases at the expense of the native form. Denaturation becomes irreversible when the refolding rate is much slower than the denaturation rate.

Modeling of reaction separation chromatography

Much experimental work has been done on the denaturation of proteins. Although denaturation may have a profound effect on protein separation, little has been done on quantitative reaction-separation modeling. Modeling has lagged behind experiments because numerical solutions and long computational times were required.

Local Equilibrium Models. Langer et al. (1969) gave a comprehensive review on the application of gas chromatography reactors to denaturation studies with emphasis on reaction kinetics but limited to linear isotherms. Karger et al. (1980) reviewed denaturation, aggregation, and many other so-called "secondary chemical equilibria" in chromatography. Keller and Giddings (1960) assumed a linear isotherm model and probability distribution between possible forms. Klinkenberg (1961) explained the band spreading in terms of slow reversible first-order reaction and rapid mass transfer (local equilibrium). Golden et al. (1974) studied selectivity reversal due to reaction in a three-component system. Villermaux (1981) studied general reaction kinetics in reaction chromatography. A detailed mathematical model for general combined separation-reaction process has been developed by Hwang et al. (1988). None of these local equilibrium models consider mass transfer and intrinsic adsorption and desorption kinetics, which are important in the separation of many large biological molecules (Muller and Carr, 1984; Lee, 1991).

Lumped Models. Endo and Wada (1983) used a stage model to consider both solution and solid phase reactions for zone-interference chromatography. Cann (1987) proposed a model to simulate simultaneous mass transfer and reaction in the hybridization and dimerization of proteins in zone electrophoresis. Whitley et al. (1989) proposed a detailed stage model, which, unlike the traditional stage model, considers interphase mass transfer and has the capability for including reaction. However, different components are assumed to have the same numbers of stages, which may not always be valid. In addition, the number of stages or overall mass-transfer coefficients have implicit dependencies on particle size, flow rate, and solute concentrations.

General Rate Models. Arve and Liapis (1987, 1988) proposed a rate model for the elution of a single adsorbate without reaction. Hsu and Ernst (1990) have proposed a reaction-separation model which considers the effects of axial dispersion. The model is solved by fast Fourier transform (FFT) method, but is limited to linear isotherms and first-order solution phase reactions. Berninger et al. (1991) developed VERSE-LC, which is a versatile reaction-separation model for liquid phase, fixed-bed adsorption. The development of this generalized model was motivated by the need for fundamental understanding of complex protein adsorption phenomena in multicomponent mixtures. Coupling of transport, intrinsic kinetics, and reaction effects often results in misinterepretation of data and adsorption mechanisms. Therefore, all the mass-transfer mechanisms (axial dispersion, film mass transfer, and intraparticle diffusion) must be accounted for properly, so that complex issues such as slow intrinsic adsorption kinetics (departure from the assumption of local equilibrium) and reaction phenomena can be thoroughly understood. Berninger et al. proposed such a set of generalized equations, initial conditions, and boundary conditions and developed a detailed solution procedure. By changing the column inlet concentration as a function of time, one can obtain dynamic solutions for any mode of adsorption operation. Many previous literature models and solutions are in fact limiting cases of this generalized model. VERSE-LC has allowed fundamental studies of a wide range of complex adsorption phenomena, including peak

compression in stepwise elution involving two-way flow (Kim et al. 1992), solute aggregation in the mobile phase (Whitley et al., 1991a; Van Cott et al., 1991), parameter estimation using gradient elution (Whitley et al., 1991b), and slow (nonequilibrium) adsorption and desorption (Whitley et al., 1993).

Research scope and key results

The focus of this article is to study adsorption phenomena due to solute denaturation. The objectives of this research are (1) to define and establish the syndrome of solute denaturation in frontal and elution chromatography; (2) to understand how the changes in particle size, flow rate, column length, gradient conditions, and column history impact separation and denaturation; (3) to design simple experiments to test whether denaturation is present; and (4) to develop strategies to minimize denaturation.

In this study, VERSE-LC is first verified with two sets of protein data for gradient elution under denaturing conditions. The simulations closely represented the data under different gradient conditions. We then use a solid phase, unimolecular, irreversible reaction to represent denaturation for isocratic and gradient elution modes, as well as for multiple cycles. The choice of this reaction is based on numerous literature observations of irreversible adsorption of proteins on hydrophobic surfaces (Beissinger et al., 1982; Andrade and Hlady, 1987). The simulations show that denaturation can result in apparent adsorption hysteresis in multiple loading-washing cycles. This phenomenon has been reported in the literature (Jennissen et al., 1987), but is simulated using a quantitative model for the first time. This study also shows that in gradient elution, peak resolution, peak elution order, and relative peak heights are all highly dependent on the gradient conditions and denaturation rates. Contrary to nonreacting systems, reducing gradient slope can actually reduce resolution in denaturation systems. A dimensionless group analysis is used to understand the conditions under which denaturation is important when design or operating parameters change. Strategies for minimizing denaturation are proposed.

Theory

Model assumptions

The following basic assumptions are used in formulating VERSE-LC:

(1) The column is packed with pseudo-homogeneous spherical particles with uniform particle size and pore size.

(2) The column has uniform flow distribution.

(3) The reaction-separation process inside the column is isothermal.

(4) The concentration gradients in the column radial direction are negligible.

(5) Angular concentration gradients in the particles are negligible.

(6) The mass-transfer coefficients are constant and independent of other components.

(7) Diffusion of solutes on the solid surface is negligible.

Model equations

Based on the above assumptions, the following governing equations can be derived from the differential mass balances for each component in the mobile, pore, and solid phases (Berninger et al., 1991):

Mobile Phase:

$$\frac{\partial c_{b,i}}{\partial \theta} = \frac{1}{Pe_{b,i}} \frac{\partial^2 c_{b,i}}{\partial x^2} - \frac{\partial c_{b,i}}{\partial x} - N_{f,i} \left(c_{b,i} - c_{p,i,\xi=1}\right) \tag{1a}$$

$$x = 0, \quad \frac{\partial c_{b,i}}{\partial x} = Pe_{b,i} \left(c_{b,i} - c_{f,i}(\theta)\right) \tag{1b}$$

$$x = 1, \quad \frac{\partial c_{b,i}}{\partial x} = 0 \tag{1c}$$

$$\theta = 0, \quad c_{b,i} = c_{b,i}(0,x) \tag{1d}$$

Pore Phase:

$$Ke_i \epsilon_p \left[\frac{\partial c_{p,i}}{\partial \theta}\right] + \frac{1}{\phi_{L,i}} Y_{\ell,i} = N_{p,i} \frac{1}{\xi^2} \frac{\partial}{\partial \xi} \left[\xi^2 \frac{\partial c_{p,i}}{\partial \xi}\right] \tag{2a}$$

$$\xi = 0, \quad \frac{\partial c_{p,i}}{\partial \xi} = 0 \tag{2b}$$

$$\xi = 1, \quad \frac{\partial c_{p,i}}{\partial \xi} = Bi_i \left(c_{b,i} - c_{p,i}\right) \tag{2c}$$

$$\theta = 0, \quad c_{p,i} = c_{p,i}(0,\xi) \tag{2d}$$

Solid Phase:

$$\frac{\partial \bar{c}_{p,i}}{\partial \theta} = Y_{\ell,i} + \bar{Y}_{p,i} \tag{3a}$$

$$\theta = 0, \quad \bar{c}_{p,i} = \bar{c}_{p,i}(0) \tag{3b}$$

Space and time are scaled by the respective characteristic values:

$$x \equiv \frac{z}{L}; \quad \xi \equiv \frac{r}{R}; \quad \theta \equiv \frac{t}{\tau}; \quad \tau \equiv \frac{L}{u_o},$$

Where τ represents the percolation time, or the time required for one bed volume of solution (excluding the particle volume) to pass through the column. The mobile, pore, and solid phase concentrations are scaled by their respective expected maximum values:

$$c_{b,i} = \frac{C_{b,i}}{C_{e,i}}; \quad c_{p,i} = \frac{C_{p,i}}{C_{e,i}}; \quad \bar{c}_{p,i} = \frac{\bar{C}_{p,i}}{\bar{C}_{T,i}}$$

where $C_{e,i}$ is the maximum possible inlet concentration for species i (assuming total conversion if there is reaction), and $\bar{C}_{T,i}$ is the maximum capacity for species i. The size exclusion factor in Eq. 2a, Ke_i, represents the fraction of the pore volume that is available to species i. Ke_i is also assumed equal to the fraction of sorbent volume available for adsorption. The $\phi_{L,i}$ is a loading factor defined as:

$$\phi_{L,i}=\frac{1}{(1-\epsilon_p)}\left[\frac{C_{e,i}}{\overline{C}_{T,i}}\right] \tag{4}$$

The $\overline{Y}_p$ term represents the consumption of species by reaction in the solid phase. The $Y_{\ell,i}$ represents the loss of component i in the pore phase by adsorption on the solid phase. Depending upon equilibrium or nonequilibrium cases, $Y_{\ell,i}$ may have different expressions, which will be discussed shortly.

Adsorption kinetics

In the model solid-phase, concentrations are related to the pore phase concentrations by means of an equilibrium isotherm or its kinetic equivalent. When the adsorption/desorption process is faster than the controlling mass-transfer and solution reaction rates, local equilibrium can be achieved between the solid and pore phases. Under such circumstances, a multiple component Langmuir isotherm has often been used for isocratic conditions (Blanco et al., 1989). For reversed-phase gradient elution, Antia and Horváth (1989) presented the reversed-phase modulator form of the Langmuir isotherm:

$$\overline{C}_{p,i}=\frac{a_i e^{-S_i\varphi}C_{p,i}}{1+\sum_{j=1}^{N_c} b_j e^{-S_j\varphi}C_{p,j}} \tag{5}$$

Snyder (1980) presents a comprehensive review of the theory behind the exponential relationship between solvent strength and retention which is included in Eq. 5. Part of the review also provides experimental verification of this model. A pair of articles by Velayudhan and Ladisch (1991, 1992) present simulation results for a system in which modulator adsorption is considered. They discuss various consequences arising from the associated gradient deformation. Isotherm information is not generally available for modulator adsorption, so we do not consider the phenomenon in this research.

If the adsorption/desorption process is relatively slow compared with the controlling mass-transfer and reaction rates, the assumption of local equilibrium is no longer valid. Consequently, solid phase concentrations must then be related to adsorption and desorption rates via a kinetic equation. A general nonequilibrium adsorption and desorption equation is presented in Whitley et al. (1993):

$$Y_{\ell,i}=N_{\ell_+,i}c_{p,i}\left[1-\sum_{j=1}^{N_c}\bar{c}_{p,j}\right]-N_{\ell_-,i}\bar{c}_{p,i} \tag{6}$$

The nonequilibrium form of Eq. 5 would then be Eq. 6 with $N_{\ell_+,i}$ and $N_{\ell_-,i}$ being dependent upon $\ell_+(\varphi)=\ell^0_+e^{-S_+\varphi}$ and $\ell_-(\varphi)=\ell^0_-e^{+S_-\varphi}$ as defined in Table 1. VERSE-LC also needs such a kinetic equation because of the way it calculates solid-phase concentrations when surface reactions are present. To reduce the number of parameters for this study, we make $N_{\ell_\pm}$ large, essentially approaching the equilibrium isotherm.

Mass-transfer parameters

The model considers four kinds of mass transfer: convection, axial dispersion (E_b), intraparticle diffusion (D_p), and film mass transfer (k_f). The axial dispersion coefficient is calculated from the correlation proposed by Chung and Wen (1968). Intraparticle diffusivity is obtained from the correlation developed by Mackie and Meares (1955). The film mass-transfer coefficient is calculated from the correlation proposed by Wilson and Geankoplis (1966). The correlations can be found together in Berninger et al. (1991). Although included in the model, axial dispersion and film mass-transfer resistance are not controlling for the systems presented.

Reaction terms

The generation or consumption of species due to reaction is represented in the governing equations by $\overline{Y}_{p,i}$:

Table 1. Dimensionless Groups

	Denominator		
Numerator	Convection	Film Mass Transfer	Intraparticle Diffusion
Axial Dispersion	$\frac{1}{Pe_{b,i}}=\frac{E_{b,i}}{u_oL}$		
Film Mass Transfer	$N_{f,i}\left(\frac{3L}{R}\right)\frac{(1-\epsilon_b)k_{f,i}}{\epsilon_b u_o}$	1	$Bi_i=\frac{k_{f,i}R}{Ke_i\epsilon_pD_{p,i}}$
Intraparticle Diffusion*	$N_{p,i}=\left(\frac{L}{R}\right)\left(\frac{1}{Pe_{p,i}}\right)$		1
Adsorption**	$N_{\ell_+,i}=\frac{L\ell_{+,i}(\varphi)C_{e,i}}{u_o}$	$Da_{\ell_+,i}=\frac{R\ell_{+,i}(\varphi)C_{e,i}}{k_{f,i}}$	$\Phi^2_{\ell_+,i}=\frac{R^2\ell_{+,i}(\varphi)C_{e,i}}{Ke_i\epsilon_pD_{p,i}}$
Desorption**	$N_{\ell_-,i}=\frac{L\ell_{-,i}(\varphi)}{u_o}$	$Da_{\ell_-,i}=\frac{R\ell_{-,i}(\varphi)}{k_{f,i}}$	$\Phi^2_{\ell_-,i}=\frac{R^2\ell_{-,i}(\varphi)}{Ke_i\epsilon_pD_{p,i}}$
Forward Reaction†	$N_{\bar{k}_+,i}=\frac{L\bar{k}_{+,m}(\varphi)}{u_o}$	$Da_{\bar{k}_+,i}=\frac{R\bar{k}_{+,m}(\varphi)}{k_{f,i}}$	$\Phi^2_{\bar{k}_+,i}=\frac{R^2\bar{k}_{+,m}(\varphi)}{Ke_i\epsilon_pD_{p,i}}$

*$Pe_{p,i}=\frac{u_oR}{Ke_i\epsilon_pD_{p,i}}$

**Equation 6 terms for nonequilibrium reversed-phase modulator equation.
†Shown for solid-phase $\overline{N}\rightarrow\overline{P}$ reaction.

$$\bar{Y}_{p,i}=\frac{L}{u_o\bar{C}_{T,i}}\sum_{m=1}^{N_r}\bar{\sigma}_{i,m}\left(\bar{k}_{+,m}\prod_{j,\text{reac}}\bar{C}_{p,j}^{-\bar{\sigma}'_{j,m}}-\bar{k}_{-,m}\prod_{j,\text{prod}}\bar{C}_{p,j}^{\bar{\sigma}'_{j,m}}\right) \quad (8)$$

where $\sigma_{i,m}$ is the coefficient of component i in the m^{th} reaction (positive for products, negative for reactants) and $\bar{k}_+$ and $\bar{k}_-$ are the forward and reverse rate constants of the reaction. For the case of an irreversible solid-phase reaction, such as surface-induced protein denaturation, the $\bar{k}_-=0$. We further treat the reaction as first-order with respect to the reactant ($\bar{\sigma}'_N=1$), so that Eq. 8 simplifies to Eq. 9 for the current study.

$$\bar{Y}_{p,N}=N_{\bar{k}_+}\bar{c}_{p,N} \quad (9)$$

Since the Gibbs free energy for protein folding changes as a linear function of cosolvent concentration, the rate "constants" actually have an exponential dependence on modulator concentration (Ahmad and Bigelow, 1986; Herskovits et al., 1970). Similar to the relationships of ℓ_+ and ℓ_-, we express this dependence as:

$$\bar{k}_{+,m}(\varphi)=\bar{k}^0_{+,m}e^{\varphi\beta_{+,m}} \quad (10)$$

where β_+ is the reaction modulator constant, which represents the dependence of reaction rate constant on the volume fraction φ of organic solvent (modulator) in the mobile phase. A large negative β_+ value imparts a faster decrease in denaturation rate with gradient progression.

Dimensionless group analysis

In complex reaction-separation systems, even a small number of components can give rise to a large number of competing mass-transfer and reaction rates. In many cases, more than one among many mass-transfer and reaction mechanisms can be controlling or affecting the observed peaks or concentration fronts. Determining these controlling steps not only can greatly simplify the problem itself, but also can show how to manipulate the complicated reaction-separation process. A fundamental engineering approach to these complex systems is to use dimensionless groups which are ratios of various rates. These groups can be classified into three categories: mass-transfer groups (Bi, N_f, N_p, Pe, Re), reaction groups ($Da_{\ell_\pm}$, $N_{\bar{k}_\pm}$, $N_{\ell_\pm}$, Φ^2) and operational or boundary groups (G, ϕ_L, $\Delta\theta$). The detailed dimensionless group tables for nongradient systems have been published elsewhere (Berninger et al., 1991).

In gradient elution mode, a new dimensionless group G, dimensionless gradient slope, is introduced to represent the gradient conditions. From the inlet boundary condition (Eq. 1b), the inlet modulator concentration of a linear gradient system can be written as:

$$\varphi_f(\theta)=\varphi_f^0+G\theta \quad (11)$$

where φ_f^0 is the initial dimensionless modulator concentration in the feed. The dimensionless gradient slope G is defined as:

$$G=\frac{\text{gradient slope}}{\text{convection rate}}=\frac{S\tau}{\varphi_e} \quad (12)$$

with S being the gradient slope and φ_e being the maximum modulator concentration. In RPLC mode, φ_s is taken to be the volume fraction of organic solvent. For linear gradients, G is a constant; in other types of gradients, G is a function of time.

Numerical solution of the governing equations

The coupled governing equations are solved by the method of orthogonal collocation on finite elements (OCFE). It involves two steps: first, the spatial axes, z and r, are discretized by OCFE; then the resulting ordinary differential equations systems with initial conditions are solved with an integrator. DASSL-A differential algebraic system solver (Petzold, 1982) is used for the VERSE-LC model. A detailed description of the scaling, assumptions, and numerical solution, including stability analysis, for VERSE-LC was presented in Berninger et al. (1991).

Results and Discussion

First, VERSE-LC is quantitatively verified by literature data on protein gradient elution. Similar parameters are then used in a series of simulations to illustrate the effects of denaturation in different modes of adsorption operations, including frontal (breakthrough curves), elution (step-down in concentration), isocratic elution of a pulse, multiple cycles, and gradient elution of a pulse. Results from different particle sizes, feed concentrations, pulse sizes, flow rates, column lengths, and gradient conditions are characterized using a dimensionless group analysis. Changes in these parameters can shift the process between reaction controlling and mass-transfer controlling as will be shown by the dimensionless group analysis.

Comparison of model predictions with literature data

Papain Denaturation on a C-4 Reversed-Phase Column. Papain did not denature in an injection solution (10 mM H_3PO_4 at pH = 2.2), but the RPLC of papain led to two peaks; the first peak is the native form, and the second peak is the denatured form (Benedek et al., 1984; Karger and Blanco, 1989). Denaturation rate increases with increasing temperature or decreasing pH. Reinjection of both peaks showed that the denaturation was irreversible under the experimental conditions of Benedek et al. (1984). Figure 1 shows the chromatograms of papain with constant surface contact time as a function of the starting mobile phase concentration (data as dashed lines). In the experiment, a four minute delay time exists for the gradient to travel from the pumping system to the column. In order to maintain the same retention time of the two peaks in the four experiments, a longer isocratic hold time was used with a higher starting propanol concentration. The slight change in gradient shape did not affect the retention times of the two peaks, but did change the relative areas. For a given contacting time, a larger native peak was observed with a higher 1-propanol fraction in the starting mobile phase. Presence of the organic solvent in the mobile phase decreases the solid phase denaturation rate.

The VERSE-LC simulated chromatograms for papain are shown as the solid line peaks in Figure 1; the simulation parameters are listed in Table 2. With only one set of parameters, four elution profiles were closely represented by simulation. Peak retention time, peak broadening, as well as relative peak

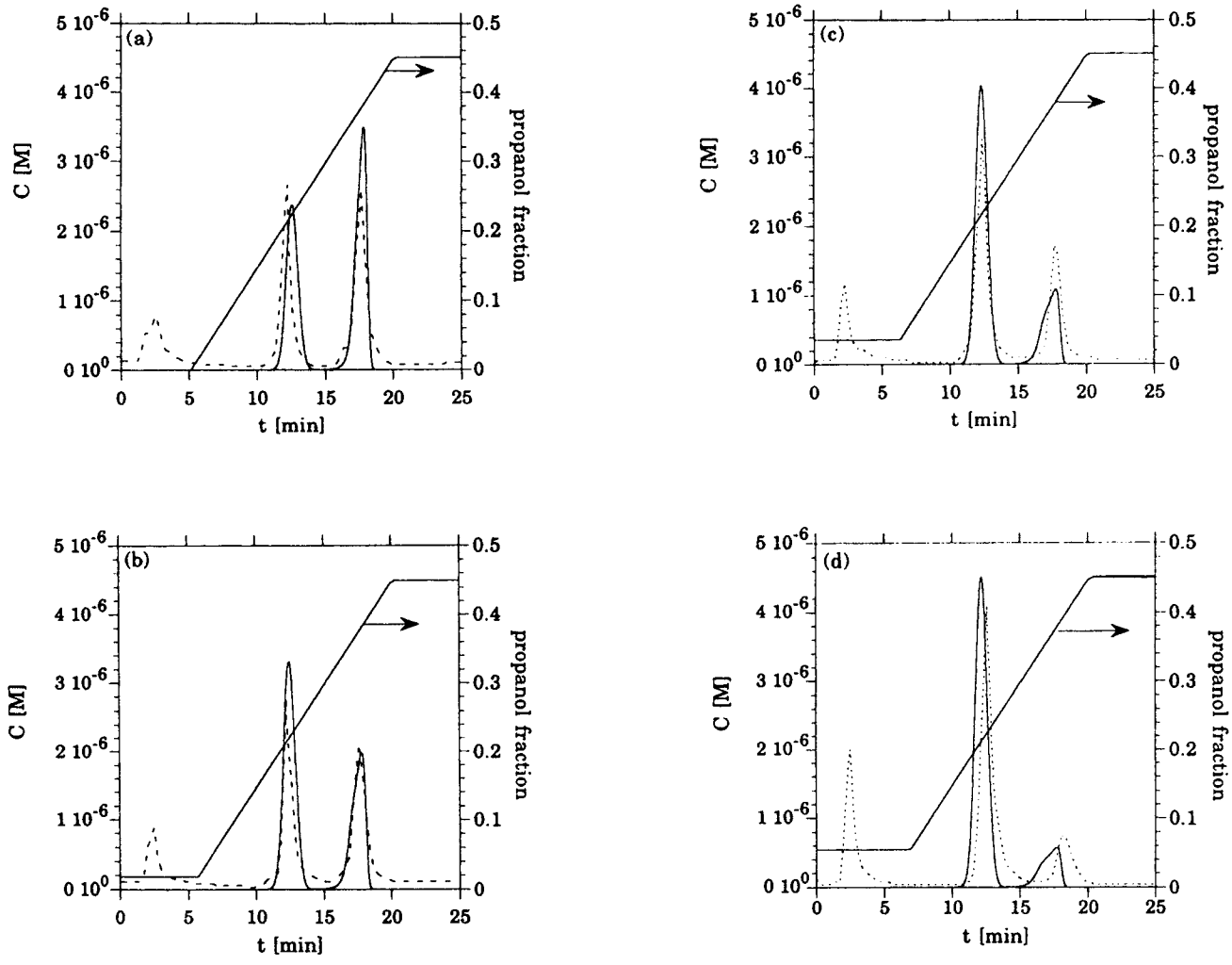

Figure 1. Model validation by gradient elution data of papain (Benedek et al., 1984, Figure 3).

First peak is native form. See Table 2 for simulation parameters. $G = 0.0388$; (a) $c^0_{f,S} = 0$; (b) 0.04; (c) 0.08; (d) 0.12; gradient durations are (a) 15.0; (b) 14.4; (c) 13.8; (d) 13.2 min.

Table 2. Parameter Values for Model Validation of Figures 1 and 2

	Isotherm*	$\ell_{+,i}$ ($M^{-1}\cdot min^{-1}$)	$\ell_{-,i}$ (min^{-1})	$S_{+,i}$	$\bar{C}_{T,i}$ (M)	$C_{P,i}$ (M)
Figure 1	N	3.65×10^5	10^3	2.3	0.07	9.662×10^{-4}
	P	7.2×10^6	10^3	11.7	0.07	0
Figure 2	N	3.5×10^5	10^3	10.0	0.07	9.09×10^{-4}
	P	5.0×10^6	10^3	11.1	0.07	0
	Reaction		$\bar{k}_{+,m}$ (min^{-1})		$\beta_{+,m}$	
Figure 1			0.17		−35.0	
Figure 2			140.0		−35.0	
	Mass Transfer		D_i^∞ ($cm^2\cdot min^{-1}$)		$D_{p,i}$ ($cm^2\cdot min^{-1}$)	
Figure 1	N,P		6.18×10^{-5}		4.0×10^{-5}	
	S		9.00×10^{-4}		2.0×10^{-4}	
Figure 2	N,P		6.12×10^{-5}		4.0×10^{-6}	
	S		9.00×10^{-4}		2.0×10^{-4}	
	System					
Figures 1, 2	ϵ_b	0.35	R (cm)	5×10^{-4}	V_p (mL)	0.006
	ϵ_p	0.5	d (cm)	0.46		
	u_o ($cm\cdot min^{-1}$)	17.19	L (cm)	10.0		

* $S_{-,i}$ is 0 for all cases.

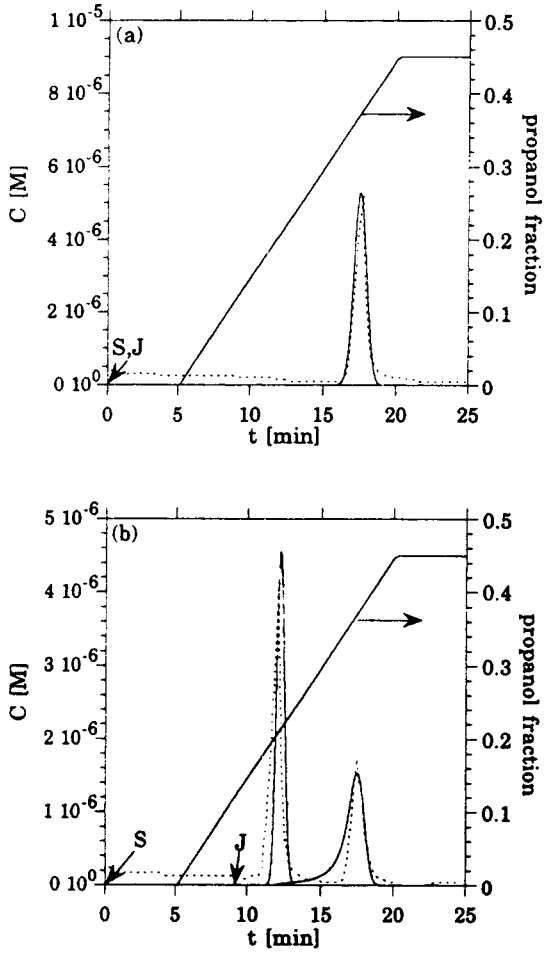

Figure 2. Model validation by gradient elution data of α-chymotrypsinogen (Benedek et al., 1984, Figure 7).

First peak is native form. See Table 2 for simulation parameters. $G = 0.0388$; $c^0_{f,S} = 0$; (a) pulse injection (J) and gradient (S) begin together; (b) injection begins 9 min. after gradient.

height, were all very close to the data. This indicates that the model can quantitatively describe the denaturation process. The largest difference between model and data is in the shape of the denatured peak for Figure 1d; VERSE-LC predicts a broader peak. Benedek et al. (1984) discuss extensively that the denaturation mechanism is composed of two steps, the first being a rapid denaturation and the second being slower (and insignificant as modulator concentration increases). Since we only consider a simple, single step denaturation process, our parameters represent an average rate. At the higher initial propanol concentration in Figure 1d, our average rate is not fast enough. Thus, the two peaks spread apart while P is still being formed causing the broader shape. The initial, rapid step in the data do not allow time for such spreading. While we could have added a second mechanism to the model, there is not enough data to accurately determine its parameters.

Parameters for model simulation were determined in the following way. The symmetrical peak shapes in the data indicate operation in the linear part of the isotherms, meaning that only a_i and S_i (see Eq. 5) are needed for N and P. These four parameters were determined using the eight retention times of the N and P peaks in Figures 1a through 1d (Schoenmakers et al., 1978). Some adjustment of D_p was also made but it was taken to be the same for N and P and independent of the modulator concentration. The denaturation rate constant ($\bar{k}_+$) and dependence of denaturation rate on modulator concentration (β_+) were then determined by matching the four relative peaks sizes in the series of experiments. Thus, a total of seven parameters can closely describe the eight peaks in all experimental chromatographs in terms of retention, peak sharpness, and peak areas for various gradient elution conditions.

α-Chymotrypsinogen Denaturation on a C-4 Reversed-Phase Column. Simulation of the chromatographic behavior of α-chymotrypsinogen as a function of injection time by VERSE-LC is shown in Figure 2; S represents the starting gradient time and J represents the sample injection time. Experimental data from Benedek et al. (1984) for this system is shown as dashed lines in Figure 2. When operated under a linear gradient from 0 to 1-propanol-water (45:55 v/v) with a constant 10 mM H_3PO_4, only a single denatured peak was observed (Figure 2a). Denaturation was dominant mainly because for the experimental system, the gradient requires 4 min. to reach the column entrance. However, upon injection 9 min. after the start of the gradient, they observed a native peak followed by a denatured peak (Figure 2b) since the protein is not exposed to the highly denaturing conditions of the starting solution. Once again, the ratio of the areas of the first peak to that of the second depended on the time of injection with the first peak growing with delayed injection. Elution time of the denatured form remained constant.

Simulations by VERSE-LC for this system are shown as solid line peaks in Figure 2; simulation parameters are listed in Table 2 and parameters were found as described for Figure 1. However, the N peak is not noticeable in Figure 2a, necessitating our assumption that it would elute at approximately the same time that it does in Figure 2b. Since the unfolding of α-chymotrypsinogen in an acid medium proceeds readily and is reversible (Herskovits et al., 1970), Benedek et al. (1984) were not able to identify the peaks by activity. However, they did show that reinjection of either fraction resulted in the appearance of both peaks, and they suggested that the second peak was the denatured form based on comparative studies (Benedek et al., 1984). Since the peaks are well separated, the

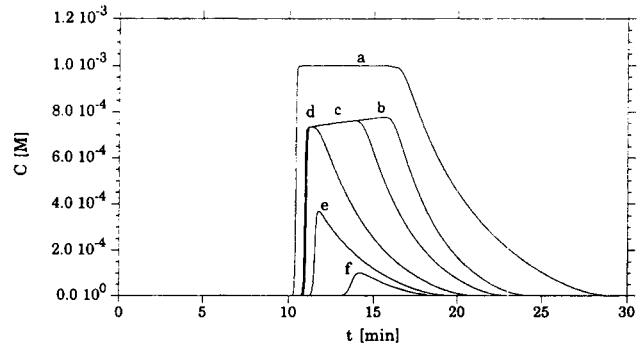

Figure 3. Impact of denaturation on volume overload elution for increasing incubation time on the column: (a) no denaturation, no incubation.

Remaining curves include (b) denaturation and incubation of 0; (c) 2; (d) 5; (e) 7.5; (f) 10 min.

solution refolding must be slow relative to the elution time so we used an irreversible solid phase denaturation in the simulation. Comparing the simulation results of Figure 2 with the experimental results, one can see that the model simulation quantitatively represents the experimental results, with the retention time, band spreading, and relative peak areas very similar to the experimental results.

Isocratic operations

As was the case for nonequilibrium adsorption kinetics (Whitley et al., 1993), denaturation can cause complications as system or operating parameters change. In this section, we will explore how common changes in process conditions can affect separations when denaturation is present. Simulation parameters are as shown in Table 3 unless otherwise noted.

Discerning Denaturation under Volume Overload. In order to maximize the throughput of a column, large pulses of dilute solutions are fed creating a condition popularly called "volume overload." Figure 3 shows a comparison of a 5 mL pulse of component N with and without denaturation. Unless a careful calibration curve was being used, one might not realize there is a significant loss of native form at $N_{\bar{k}_+} = 0.125$ (Figure 3, curve b). However, if one runs the same experiment with a short incubation period (stopped flow for a period of time after pulse injection), the area under the curve would decrease and a comparison could be made. The series of increasing incubation times (curves c to f) indicate how much protein is being left on the column. The incubation times have been subtracted from the time values so that the curves overlay for comparison purposes. The "roll-up" or positive slope at the top of the b-d curves is also indicative of competition with a reactant; note that curve a has a horizontal plateau. Minimizing residence time and gradient delay is necessary to minimize denaturation.

Differentiating Between Solution and Solid-Phase Denaturation. One can incubate samples before injection for a series of times. If this makes a difference in the effluent history, solution phase denaturation should be suspected. In contrast, incubation of material on the column will alter the effluent history if solid-phase denaturation is present.

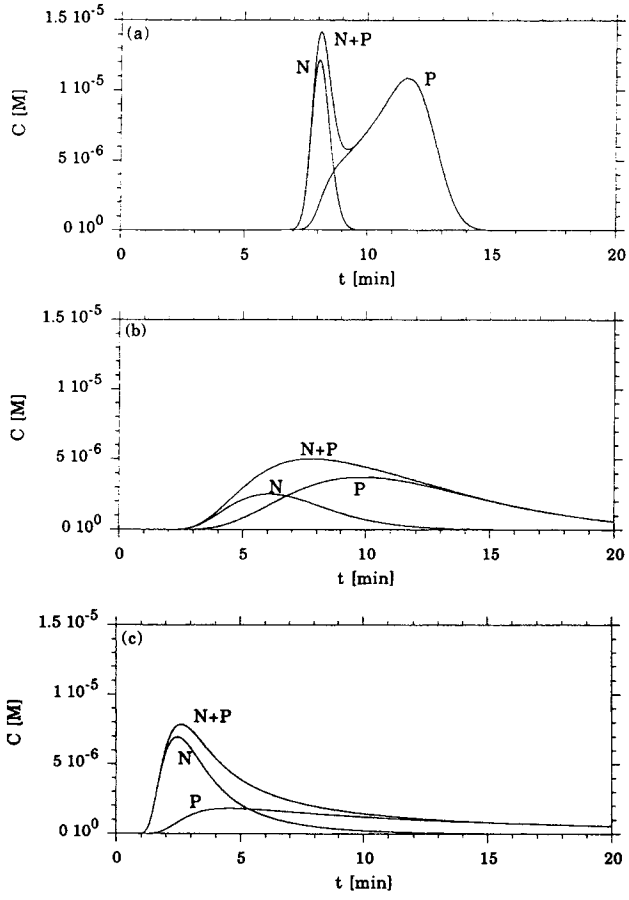

Figure 4. Effects of particle size in isocratic elution ($N_{\bar{k}_+} = 0.5$).

$C_{P,N} = 10^{-4}M$; $V_{P,N}$ 0.5 mL; (a) $R = 5\times10^{-4}$; (b) 5×10^{-3}; and (c) 1.5×10^{-2} cm; (a) $\Phi^2_{\bar{k}_+} = 8.375\times10^{-3}$; (b) 0.8375; and (c) 7.54.

Effects of Changing Particle Size. Large particles are often used in preparative scale chromatography to minimize pressure drop in longer beds. Figure 4 shows the effects of changing particle size. As the particle radius increases from 5×10^{-4} cm

Table 3. Parameter Values for Isocratic Simulations (Figures 3-8)

Figure	Isotherm*	$\ell_{+,i}$ ($M^{-1}\cdot min^{-1}$)	$\ell_{-,i}$ (min^{-1})	$\bar{C}_{T,i}$ (M)
4-7	N	1.0×10^6	1.0×10^3	0.01
	P	2.0×10^6	1.0×10^3	0.01
7	I	see figure	1.0×10^3	0.01
3,8	N	1.0×10^6	1.0×10^3	0.03
	P	1.0×10^3	1.0×10^{-3}	0.03
	I	1.5×10^6	1.0×10^3	0.03
	Reaction		$\bar{k}_{+,m}$ (min^{-1})	
4-7			0.33506	
3,8			0.083765	
	Mass Transfer		D_i^∞ ($cm^2\cdot min^{-1}$)	$D_{p,i}$ ($cm^2\cdot min^{-1}$)
3-8	N,P,I		3.449×10^{-5}	1.2346×10^{-5}
	System			
3-8	ϵ_b	0.38	R (cm)	5×10^{-4}
	ϵ_p	0.81	d (cm)	1.0
	u_o ($cm\cdot min^{-1}$)	3.3506	L (cm)	5.0

* $S_{+,i} = S_{-,i} = 0$ for Figures 3-8

(curve a) to 1.5×10^{-2} cm (curve c), the intraparticle diffusion resistance becomes more important. As a result, both the native and denatured peaks become less concentrated. Because the column loses resolution power with large particle size, the denaturation effects (split peaks) are masked by the mass-transfer effects. Dimensionless group analysis is also important in predicting peak splitting and peak merging in this case. Instead of $N_{\bar{k}_-}$ being the key group as was the case for analytical scale chromatography, $\Phi^2_{\bar{k}_-}$ is the key group in the large scale. As particle radius increases from 5×10^{-4} cm to 1.5×10^{-2} cm, $\Phi^2_{\bar{k}_-}$ increases from 8.375×10^{-3} to 7.54, giving a higher effective reaction rate. Similar to the analysis in analytical chromatography, at a relatively slow reaction rate the peaks tend to separate, while at a high reaction rate the peaks tend to merge. One can also see that as intraparticle resistance becomes higher, as indicated by N_p decreasing from 60 (a) to 0.066 (c), the dynamic capacity drops. Solute molecules do not have time to penetrate very far into the large particles, so fewer binding sites are accessed, and the entire pulse shifts towards earlier elution.

Effects of Feed Concentration and Flow Rate. Increasing feed concentration increases the degree of saturation, as expressed by the loading factor, shifting the isotherm from the linear to the nonlinear region. Therefore, breakthrough occurs earlier and the front is sharper (Figure 5). For example, at a lower feed concentration ($C_{f,N} = 2.5 \times 10^{-4}$ M or $\phi_{L,N} = 0.13$, Figure 5a), the breakthrough curve shows a slower approach to saturation and two concentration waves; while at a higher concentration ($C_{f,N} = 5.0 \times 10^{-3}$ M or $\phi_{L,N} = 2.63$, Figure 5c), the breakthrough curve becomes apparently sharp. Higher feed concentration of a protein actually reduces denaturation because the residence time is much shorter. If increasing feed concentration is not practical, one can limit denaturation by increasing the flow rate. Figure 5d is identical to 5a, except that the flow rate has been doubled. Denaturation is decreased because contact time is reduced, as noted by $N_{\bar{k}_-}$ decreasing from 0.5 (5a) to 0.25 (5d). The proportion of the two species would not have changed if there was no reaction present. However, since the overall breakthrough front may not change either, a diode array detector on the effluent would be necessary to test for changes in concentration ratios.

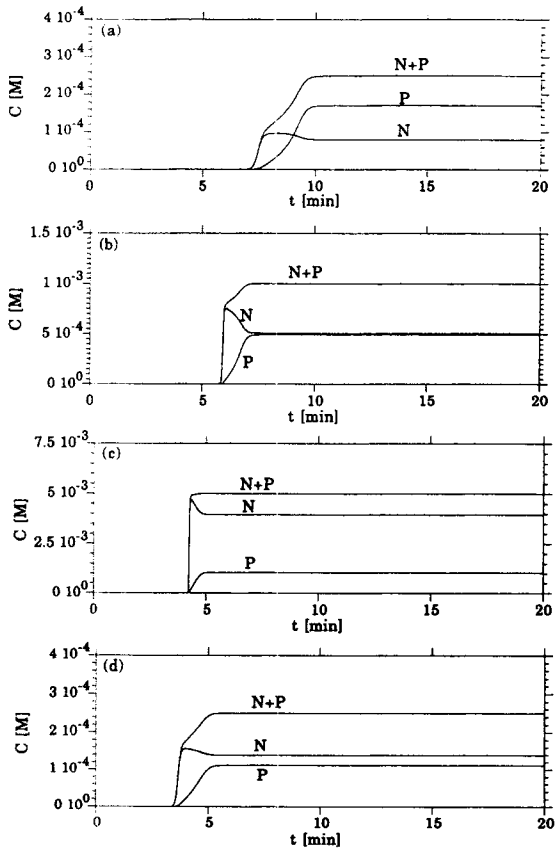

Figure 5. Reduction of denaturation by increasing feed concentration in frontal analysis ($N_{\bar{k}_+} = 0.5$).

(a) $\phi_{L,N} = 0.13$; (b) 0.53; (c) 2.6; or (d) increasing flow rate $N_{\bar{k}} = 0.25$ for $\phi_{L,N} = 0.13$.

Effects of Loading. Loading is an important parameter in elution and will influence both reaction and separation. In analytical chromatography, a small pulse (20–50 μL) can be used to eliminate loading effects, because the main purpose of analytical chromatography is high resolution. But in preparative scale chromatography, a large pulse is usually preferred in order to increase the productivity. In the case without mass-transfer or reaction effects, local equilibrium theories in the literature have established that a single component chromatogram is only a function of T (Helfferich and Klein, 1970). A dimensionless pulse size:

$$\Delta T_{o,i} = \frac{C_{e,i} u_o \Delta t_i}{(1-\epsilon_b)(1-\epsilon_p)\overline{C}_{T,i} L} \tag{11}$$

where Δt_i is pulse time, L is column length, and u_o is interstitial velocity, thus proves useful for considering both concentration and pulse volume overload. When columns are sufficiently long ($\Delta T_{o,i}$ much less than unity), the resulting peak from volume overload and concentration overload becomes identical for Langmuir isotherms in the absence of reaction (Helfferich and Carr, 1993). For low loading ($\Delta T_{o,i} < 0.01$), there are no significant pulse size effects. But at high loading, the results are different. Figure 6 shows the nonlinear region from $\Delta T_{o,N} = 0.114$ (a) to 1.14 (b, both sets) to 45.5 (c). There are two simulations in Figure 6b; the first is a 0.2 mL pulse of 0.01 M (concentration overload) and the second is a 2 mL pulse of 0.001 M (volume overload). Even though loading is the same (as noted by $\Delta T_{o,N}$), the effluent history for concentration overload is quite different from that of volume overload. While this difference is partly because the column is not exceedingly long (5 cm), the presence of a denaturation reaction is also reducing the accuracy of $\Delta T_{o,i}$ in predicting histories. Going to Figure 6c, one sees that high concentration and large pulse volumes result in merging of reactant forms and less time on the column for denaturation. The $\Delta T_{o,i}$ gives a clear indication of whether there are nonlinear effects, but does not guarantee equivalency between various combinations of pulse size and concentration when reactions such as denaturation are present.

Interference Coupled with Denaturation. Coupling of interference phenomena to the denaturation process adds another layer of complexity to the elution profiles. Simulations are useful in sorting out the interplay of these elements. Figure 7 shows the breakthrough curves of a protein mixture being separated by chromatography as one of the components under-

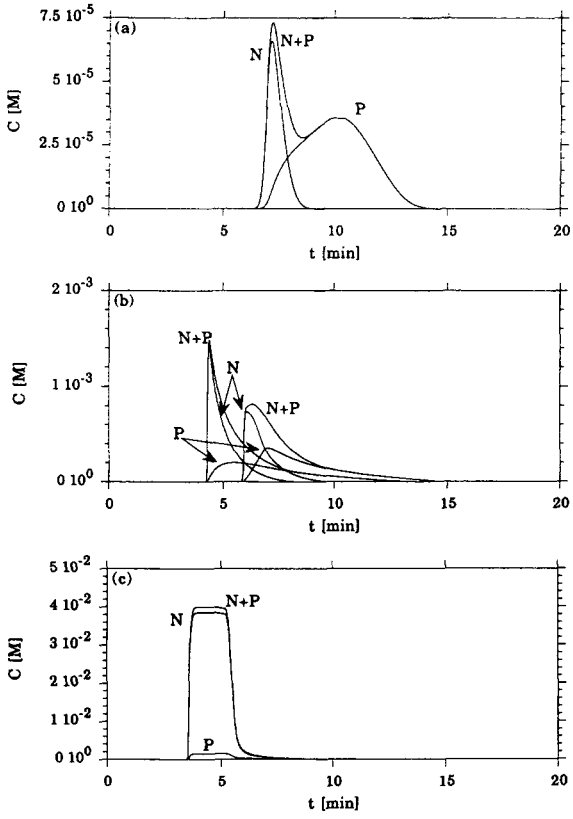

Figure 6. Effects of pulse concentration and volume on denaturation ($N\ \bar{k}_+ = 0.5$).

(a) $C_{P,N} = 0.001$; 0.01 (b, first peak set); 0.001 (b, second peak set); (c) 0.04 m; (a) $V_{P,N} = 0.2$; 0.2 (b, first peak set); 2 (b, second peak set); (c) 2 mL; (a) $\Delta T_{o,N} = 0.114$; (b) 1.14; (c) 45.5.

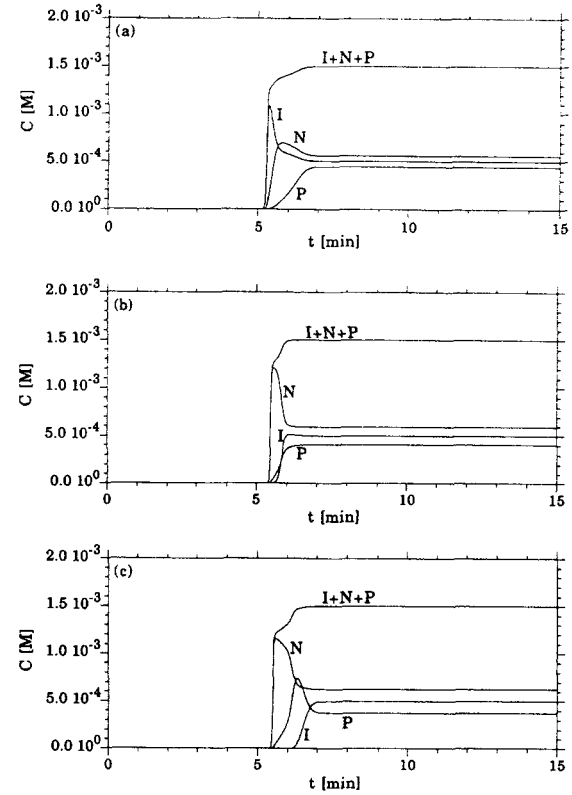

Figure 7. Impact of interference from other solutes on denaturation of a protein.

(a) $\ell_{+,I} = 8 \times 10^5$; (b) 1.5×10^6; and (c) 2.2×10^6 $M^{-1}min^{-1}$; $C_{f,N} = 10^{-3}$; $C_{f,I} = 5 \times 10^{-4}$ M for all cases.

goes denaturation. In Figure 7a, the affinity of the inert species, I, is slightly less than that of the native form. As a consequence, I is sharpened by interference from N. In Figure 7b, I has an affinity between the native and denatured forms. N has been sharpened by interference from I, and P also shows some sharpening. While in Figure 8c, I has an affinity slightly less than that of P. Compared with Figure 7b, peak P is now much sharper. Looking through this series, one should note that as the affinity of I increases, the ratio of N to P increases. Since I becomes a better competitor for sites, N spends less time on the solid phase and thus denatures less. Without multiwavelength monitoring, one may not realize there is denaturation present in addition to the expected separation of N and I because the overall curve shape which might be shown by single wavelength absorption ($I+N+P$ curve) does not change greatly.

Effects of Column History. Because of their high cost, adsorbent columns on both lab and industrial scales are subjected to repeated process cycling. Often there is a "break-in period" whereupon some (usually small) percentage of adsorbent sites irreversibly bind solutes (Regnier, 1984). For subsequent cycles, the elution times are constant. If denaturation is present and the denatured form is very strongly retained, the available capacity of the column may continue to decrease. Such a case is demonstrated by VERSE-LC in Figure 8. Throughout four successive cycles of a large pulse of $N+I$, the column loses capacity as $\overline{N}$ denatures to $\overline{P}$ which tends to stay bound to the solid phase. The loss of capacity reduces resolution between the N and I species. Additionally, the amount of "roll up" of N caused by displacement from I decreases. Displacement effect requires binding sites, some of which P takes out of use on each cycle. Detailed modeling can be useful in developing loading and regeneration steps to reduce loss of capacity due to strongly adsorbing species and to prolong column life.

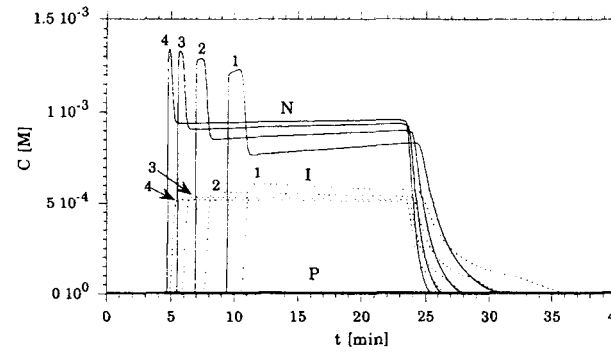

Figure 8. Multicomponent interference and loss of capacity due to solid phase irreversible denaturation.

Denatured form has slow adsorption/desorption kinetics and high affinity. Four successive cycles of a large rectangular pulse are shown. $C_{P,N} = 0.001$ M; $C_{P,I} = 0.005$ M; $V_{P,N} = V_{P,I} = 20$ mL.

Implications of denaturation of gradient elution systems

Gradient elution is widely used in chromatographic separation. The solute affinity, adsorption, and desorption rates, as well as denaturation and refolding rates, all can change with gradient conditions. This makes the modeling of protein denaturation under gradient elution conditions quite a challenge. Gradient simulation parameters for Figures 9–12 are given in Table 4 unless otherwise noted.

Selecting Flow Rate and Column Length to Reduce Denaturation. For small particle columns, the two key dimensionless groups are G and $N_{\bar{k}_+}$. Increasing column length from 1 cm (Figure 9a) to 10 cm (Figure 9c) will increase $N_{\bar{k}_+}$ from 0.0385 to 0.385; therefore, it also increases the size of the denatured peak. Also, G increases with increasing column length, resulting in a sharper peak of the denatured form, despite the increasing retention time (Figures 9a through 9c). Decreasing flow rate will have the same impact on G and $N_{\bar{k}_+}$ as increasing column length. Figure 9d shows the result when both the flow rate and the gradient slopes are doubled while holding G the same as that in Figure 9c. The peak of the denatured form becomes smaller as a result of the 50% reduction in $N_{\bar{k}_+}$, but peak sharpness remains similar to that of Figure 9c because G is kept constant.

Reversal of Peak Elution Order by Changing Gradient Conditions. Since native and denatured species can have different isotherm behavior, their elution order can also be reversed as has been demonstrated experimentally by Kunitani et al. (1986) in RPLC. By changing gradient conditions, we can get separated peaks or a single peak or a change in the elution order. Figure 10 shows a series with different gradient slopes, while all other conditions are the same. In Figure 10a a sharp gradient is chosen ($G=0.0349$) and the denatured form elutes before the native form; in Figure 10b a less steep gradient is used ($G=0.0117$), and the native and denatured form merge into one peak; in Figure 10c, a shallow gradient is imposed ($G=0.00873$) and the denatured peak comes out after the native peak. Figure 10 demonstrates two important points about gradients under denaturing conditions: (1) decreasing gradient slope can sometimes decrease resolution, and (2) the peak elution order can change with G.

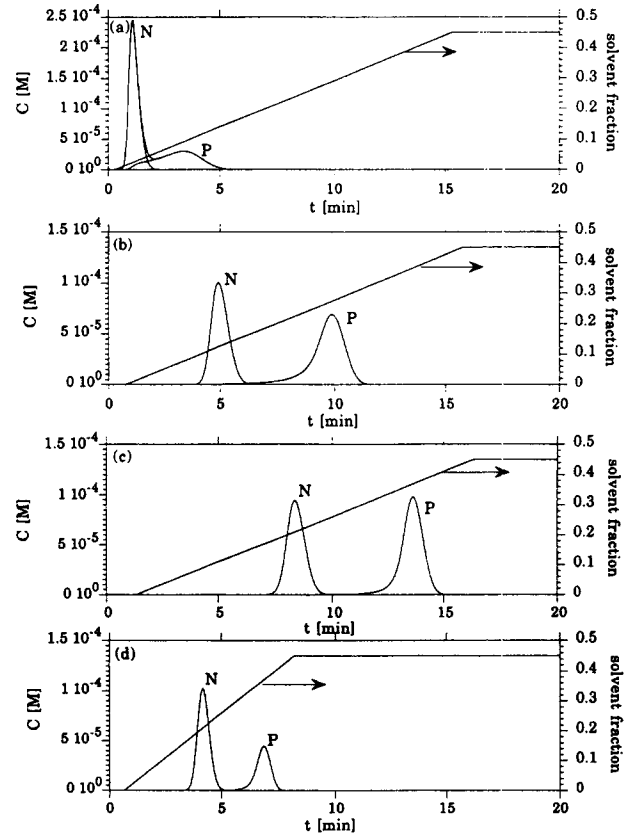

Figure 9. Selection of column length and flow rate for resolution and reduction of denaturation.

(a) G = 0.00388; (b) 0.0194; (c) 0.0388; (d) 0.0388; (a) $N_{\bar{k}_+}$ = 0.0385; (b) 0.1925; (c) 0.385; (d) 0.1925; $\Delta T_{o,N}$ = 0.275; $c^0_{f,S}$ = 0; gradient starts at end of pulse.

Effects of Adsorption Modulator Constant (S_+). Figure 11 shows how the modulator constant S_+ in Eq. 6 can affect the separation and elution order of native and denatured forms. In Figure 11, $S_{+,N}$ is kept constant while $S_{+,P}$ increases from 6.9 to 25.0. The denatured peak becomes sharper and elutes

Table 4. Parameter Values for Gradient Simulations (Figures 9–12)

Figure	Isotherm*	$\ell_{+,i}$ ($M^{-1}\cdot min^{-1}$)	$\ell_{-,i}$ (min^{-1})	$S_{+,i}$	$\bar{C}_{T,i}$ (M)	
9-12	N	6.0×10^4	1.0×10^2	4.5	0.03846	
	P	3.0×10^5	1.0×10^2	6.9	0.03846	
10	N	6.0×10^4	1.0×10^2	4.5	0.03846	
	P	3.0×10^5	1.0×10^2	15.0	0.03846	
11	N	6.0×10^4	1.0×10^2	4.5	0.03846	
	P	3.0×10^5	1.0×10^2	see figure	0.03846	
	Reaction		$\bar{k}^o_{+,m}$ (min^{-1})		$\beta_{+,m}$	
9-11			0.6619		−30.0	
12			0.6619		see figure	
	Mass Transfer		D_i^∞ ($cm^2\cdot min^{-1}$)		$D_{p,i}$ ($cm^2\cdot min^{-1}$)	
9-12	N,P		1.1304×10^{-4}		2.512×10^{-5}	
	S		9.00×10^{-4}		2.00×10^{-4}	
	System					
9-12	ϵ_b	0.35	R (cm)	5×10^{-4}	$V_{P,N}$ (mL)	0.2
	ϵ_p	0.50	d (cm)	0.46	$C_{P,N}$ (M)	10^{-3}
	u_o ($cm\cdot min^{-1}$)	17.192	L (cm)	10.0		

* $S_{-,i}$ is 0 for all cases.

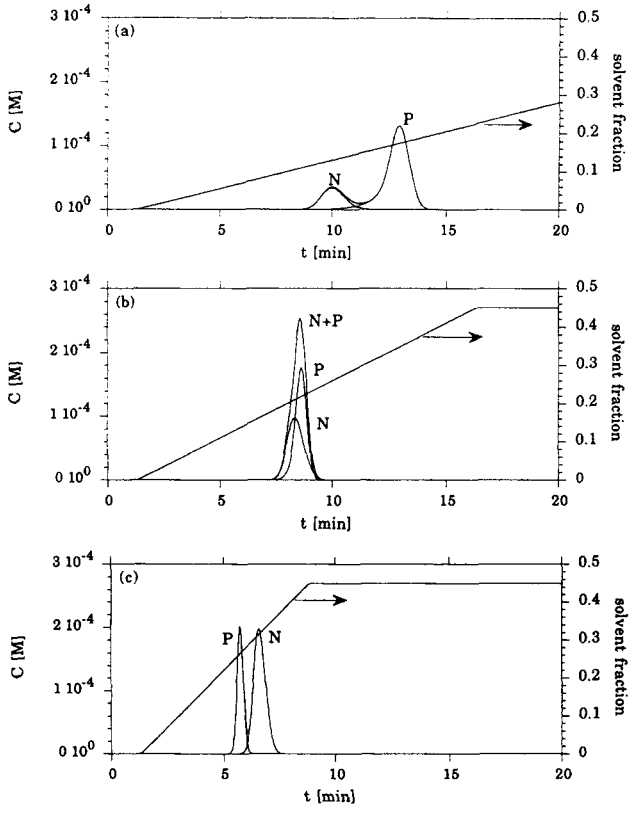

Figure 10. Reversal of peak elution order by increasing gradient slope ($N_{\bar{k}_+}$ = 0.385, affinity modulator constant $S_{+,N}$ = 4.5, $S_{+,P}$ = 15.0).

(a) $G = 0.0194$; (b) 0.0388;(c) 0.0776; $c^0_{f,S} = 0$; gradient starts at 0.2 min.

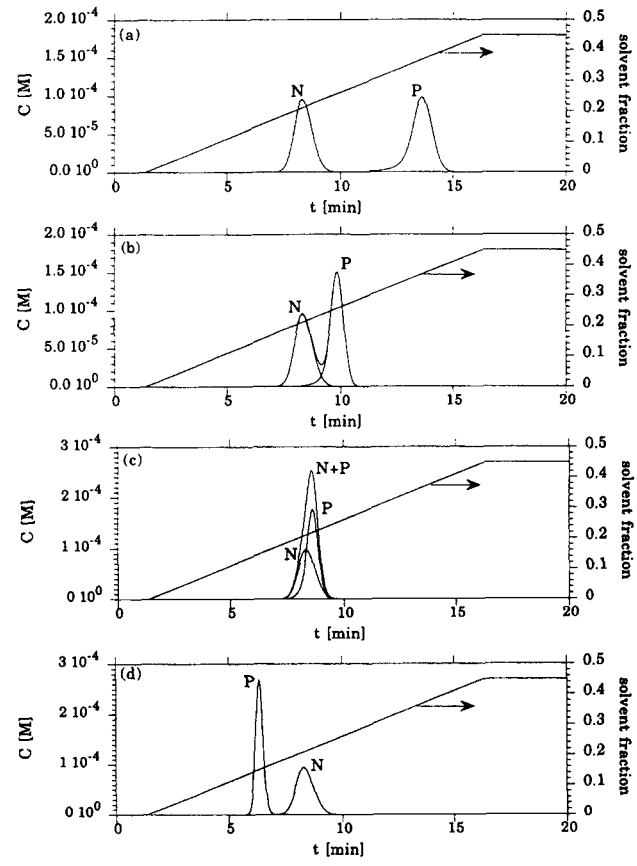

Figure 11. Effects of changing affinity modulator constant, (a) $S_{+,P}$ = 6.9; (b) 12; (c) 15; (d) 25.

$G = 0.0388$; $c^0_{f,S} = 0$; gradient starts at 0.2 min.

earlier as $S_{+,P}$ increases. Keeping all other parameters constant, different $S_{+,P}$ can sometimes cause the denatured form to come out later than the native form (Figure 11a, 11b); sometimes they can merge into one peak (Figure 11c); in an extreme case, the denatured form can elute before the native form (Figure 11d). As a general rule, denatured forms come out after native forms. This and the previous figure results show that this may not always be the case. Hence, a biological activity assay or other tests are needed to determine which peak is due to the denatured form.

Effects of Reaction Rate Modulator Constant (β_+). The denaturation rate constant, β_+, is often affected by the mobile phase conditions (Benedek et al., 1984). Figure 12 shows a series of chromatograms with different β_+. Basically, β_+ has two important effects on the chromatogram. First, it can change the relative peak heights of the native and denatured species. A more negative value for β_+ means the reaction rate slows down more quickly as the gradient progresses, resulting in less denatured species. That is why there is less denatured form in Figure 12c ($\beta_+ = -30$) than in Figure 12b ($\beta_+ = -10$). Second, β_+ can affect resolution between the native and denatured peaks. Figure 12a shows a case where β_+ equals 0, which means the reaction rate is independent of gradient conditions. In this case, the denatured peak is spread-out, distorted, and not fully separated from the native peak. For many systems reported in the literature, such distorted peaks were not observed, indicating denaturation rate is usually a function of φ.

Since protein denaturation in RPLC and HIC is mainly due to the hydrophobicity of the sorbent surface, which turns the inner hydrophobic part of a protein out, it should be expected that injection of a protein sample into a mobile phase containing some organic solvent can reduce denaturation. However, if the mobile phase organic solvent concentration is too high, protein can denature in the mobile phase as well (Kerlavage et al., 1983). The combination of solution and solid phase denaturation is not included in the simulations because no quantitative experimental data are presently available for bench marking.

Conclusions

A comprehensive liquid chromatography model has been extended to describe the effects of protein denaturation in frontal chromatography and in nonlinear isocratic and gradient elution chromatography. The model has been verified with RPLC literature data of papain and α-chymotrypsinogen. In the papain simulations, one set of parameters closely represents four gradient elution profiles (8 peaks) showing denaturation as a function of hold time. In the α-chymotrypsinogen simulations, one set of parameters closely represented native and denatured peaks for two different injection times under gradient.

In frontal chromatography, denaturation results in multiple waves or asymmetric breakthrough curves, which can be mis-

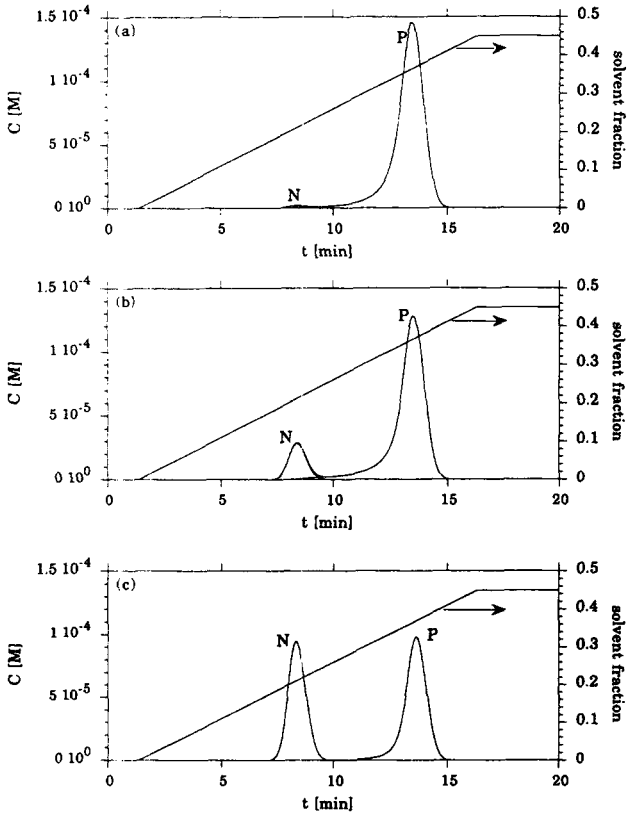

Figure 12. Effects of changing reaction rate modulator constant, (a) $\beta_+ = 0$; (b) -10; and (c) -30.

$G = 0.0388$; $c^0_{f,S} = 0$; gradient starts at 0.2 min.

takenly attributed to impurities. However, data at increasing flow rate can differentiate the effects due to impurities from those due to denaturation. Multiwavelength detection may be needed, however, since overall front shapes may not change.

In isocratic elution, peaks of native and denatured forms cannot be fully separated because of the denaturation reaction. Surface induced denaturation can also be detected by incubation adsorbed samples for different periods of time, followed by elution. Introduction of an interfering component to a denaturing system was shown to modulate the rate of solid phase denaturation by occupying some of the denaturing sites. If the denatured species is irreversibly bound, repeated cycling will show apparent adsorption hysteresis and loss of capacity.

The model showed that a higher flow rate or a shorter column length will reduce the degree of denaturation due to exposure to sorbents, but of course harm resolution. Using larger particles to reduce column pressure drop also reduces resolution by causing additional band spreading. The result is a higher effective reaction rate which masks denaturation. Peak splitting due to denaturation is more pronounced at low feed concentrations than at high concentrations. At nonlinear isotherm concentrations, an increase in pulse size will cause the splitting peaks to merge into one peak with a sharp front and long tailing.

In gradient elution, peak resolution, peak elution order, and relative peak heights are all highly dependent on the gradient conditions. Resolution between the two forms can be aided by longer columns or slower flow rates. Greater dependence of denaturation rate on the mobile phase (more negative β_+) gives sharper peaks and can also improve resolution between native and denatured peaks. Contrary to nonreacting systems, reducing gradient slope can actually reduce resolution in denaturation systems if the potential for peak reversal is present. The normal elution order of native form before denatured form can be reversed by a large adsorption modulator constant for the denatured form or by a change in the gradient slope and flow rate. Thus, a biological activity assay or other analysis may be needed for identification of the peaks.

Acknowledgment

This work was supported by National Science Foundation through grants BCS-8912150 and BCS-9007785. The authors are grateful to James A. Berninger and Xue-Zhi Jin for helpful discussions.

Notation

a = isotherm parameter, M(solid) M(pore)$^{-1}$
b = isotherm parameter, M(pore)$^{-1}$
Bi = Biot number
c = dimensionless concentration
C = concentration, M
C_T = capacity of exchanger, M(solid)
D^∞ = Brownian diffusivity, cm^2·min^{-1}
D_p = effective intraparticle diffusivity, cm^2·min^{-1}
$Da_{t_\pm}$ = Damköhler number; ratio of adsorption/desorption rate to film mass-transfer rate
E_b = axial dispersion coefficient, cm^2·min^{-1}
G = dimensionless gradient slope, defined by Eq. 12
I = nonreacting molecular species
k_+ = reaction rate constant, min^{-1}
k_f = film mass-transfer parameter, cm·min^{-1}
Ke = size exclusion factor
ℓ_+ = reaction rate constant of adsorption, M(pore)$^{-1}$min^{-1}
ℓ_- = reaction rate constant of desorption, min^{-1}
L = column length, cm
N = molecular species
N_c = number of components
N_f = ratio of film mass-transfer rate to convection rate
N_{k_+} = ratio of (solid phase) reaction rate to convection rate
$N_{\ell_\pm}$ = ratio of adsorption/desorption rate to convection rate
N_p = ratio of diffusion rate to convection rate
N_r = number of reactions
P = molecular species
Pe = Peclet number
r = particle position, cm
R = particle radius, cm
Re = Reynolds number
S = gradient slope, min^{-1}
$S_\pm$ = adsorption/desorption modulator constant
t = time, min
u_o = interstitial velocity, cm·min^{-1}
V = volume of input pulse, mL
x = dimensionless column position
Y = generation term
z = column position, cm

Subscripts

b = bulk phase
e = maximum inlet concentration
f = current inlet concentration
i,j = component counters
m = reaction counter
p = particle phase
P = relating to input pulse
T = loading term for pulse input

Superscripts

- $\bar{}$ = solid phase
- * = equilibrium isotherm simulation
- ^{0} = initial or limiting value

Greek letters

- β = reaction modulator constant
- Δ = change
- ϵ_b = interparticle void fraction
- ϵ_p = intraparticle porosity
- θ = dimensionless time
- ξ = dimensionless particle position
- σ = coefficient of component in reaction equation
- $\bar{\sigma}'$ = solid-phase reaction order
- τ = percolation time, min
- φ = modulator fraction
- ϕ_L = loading factor
- Φ^2 = Thiele modulus

Literature Cited

Ahmad, F., and C. C. Bigelow, "Thermodynamic Stability of Proteins in Salt Solutions: A Comparison of the Effectiveness of Protein Stabilizers," *J. Protein Chemistry*, **5**(5), 355 (1986).

Andrade, J. D., "Principles of Protein Adsorption," in *Surface and Interfacial Aspects of Biomolecular Polymers*, Vol. 2, *Protein Adsorption*, J. D. Andrade, ed., Plenum Press, New York (1985).

Andrade, J. D., and V. Hlady, "Plasma Protein Adsorption: The Big Twelve," *Annal. New York Acad. Sci.*, **516**, 158 (1987).

Antia, F. D., and Cs. Horváth, "Gradient Elution in Non-linear Preparative Liquid Chromatography," *J. Chromatogr.*, **484**, 1 (1989).

Arve, B. H., and A. I. Liapis, "Modeling and Analysis of Elution Stage of Biospecific Adsorption in Fixed Beds," *Biotechnol. Bioeng.*, **30**, 638 (1987).

Arve, B. H., and A. I. Liapis, "Biospecific Adsorption in Fixed and Periodic Countercurrent Beds," *Biotechnol. Bioeng.*, **32**, 616 (1988).

Benedek, K., S. Dong, and B. L. Karger, "Kinetics of Unfolding of Proteins on Hydrophobic Surfaces in Reversed-phase Liquid Chromatography," *J. Chromatogr.*, **317**, 227 (1984).

Berninger, J. A., R. D. Whitley, X. Zhang, and N.-H. L. Wang, "A Versatile Model for Simulation of Reaction and Non-Equilibrium Dynamics in Multicomponent Fixed-Bed Adsorption Processes," *Computers Chem. Eng.*, **15**(11), 749 (1991).

Beissinger, R. L., and E. F. Leonard, "Sorption Kinetics of Binary Protein Solutions: General Approach to Multicomponent Systems," *J. Colloid Interface Sci.*, **85**(2), 521 (1982).

Blanco, R., A. Arai, N. Grinberg, D. M. Yarmush, and B. L. Karger, "Role of Association on Protein Adsorption Isotherms: β-lactoglobulin A Adsorbed on a Weakly Hydrophobic Surface," *J. Chromatog.*, **482**, 1 (1989).

Cann, J. R., "Theory of Electrophoresis of Hybridizing Enzymes with Kinetic Control: Implications for Population Genetics of Electrophoretic Markers," *J. Theor. Biol.*, **127**, 461 (1987).

Chung, S. F., and C. Y. Wen, "Longitudinal Dispersion of Liquid Flowing Through Fixed and Fluidized Beds," *AIChE J.*, **14**(6), 857 (1968).

Cohen, S. A., K. P. Benedek, S. Dong, Y. Tapuhi, and B. L. Karger, "Multiple Peak Formation in Reversed-Phase Liquid Chromatography of Papain," *Anal. Chem.*, **56**, 217 (1984a).

Cohen, K. A., K. Schellenberg, K. Benedek, B. L. Karger, B. Grego, and M. T. W. Hearn, "Mobile-Phase and Temperature Effects in the Reversed-Phase Chromatographic Separation of Proteins," *Anal. Biochem.*, **140**, 223 (1984b).

Cohen, S. A., K. Benedek, Y. Tapuhi, J. C. Ford, and B. L. Karger, "Conformational Effects in the Reversed-Phase Liquid Chromatography of Ribonuclease A," *Anal. Biochem.*, **144**, 275 (1985).

Endo, S., and A. Wada, "Theoretical and Experimental Studies on Zone-Interference Chromatography as a New Method for Determining Macromolecular Kinetic Constants," *Biophys. Chem.*, **18**, 291 (1983).

Golden, F. M., K. I. Shiloh, G. Klein, and T. Vermeulen, "Theory of Ion-Complexing Effects in Ion-Exchange Column Performance," *J. Phys. Chem.*, **78**, 926 (1974).

Hearn, M. T. W., and B. Grego, "High-Performance Liquid Chromatography of Amino Acids, Peptides and Proteins. LV. Studies on the Origin of Band Broadening of Polypeptides and Proteins Separated by Reversed-Phase High-Performance Liquid Chromatography," *J. Chromatog.*, **296**, 61 (1984).

Hearn, M. T. W., and M. I. Aguilar, "High-Performance Liquid Chromatography of Amino Acids, Peptides and Proteins: LXXIII. Investigations on the Relationships Between Molecular Structure, Retention and Band-Broadening Properties of Polypeptides Separated by Reversed-Phase High-Performance Liquid Chromatography," *J. Chromatog.*, **397**, 47 (1987).

Helfferich, F. G., and G. Klein, *Multicomponent Chromatography. Theory of Interference*, Marcel Dekker, New York (available from University Microfilms International, Ann Arbor, MI, #2050382) (1970).

Helfferich, F. G., and P. W. Carr, "Nonlinear Waves in Chromatography. I. Waves, Shocks, and Shapes," *J. Chromatog.*, **629**, 97 (1993).

Herskovits, T. T., B. Gadegbeku, and H. Jaillet, "On the Structural Stability and Solvent Denaturation of Proteins, I. Denaturation by the Alcohols and Glycols," *J. Biol. Chem.*, **245**, 2588 (1970).

Hsu, J. T., and U. P. Ernst, "Theoretical Studies of Reaction Chromatograms by the Fast Fourier Transform Technique," *Chem. Eng. Sci.*, **45**(4), 1017 (1990).

Hwang, Y.-L., F. G. Helfferich, and R. J. Leu, "Multicomponent Equilibrium Theory for Ion-Exchange Columns Involving Reactions," *AIChE J.*, **34**(10), 1615 (1988).

Ingraham, R. H., S. Y. M. Lau, A. K. Taneja, and R. S. Hodges, "Denaturation and the Effects of Temperature on Hydrophobic-Interaction and Reversed-Phase High-Performance Liquid Chromatography of Proteins. Bio-Gel TSK-Phenyl-5-PW Column," *J. Chromatog.*, **327**, 77 (1985).

Jacobson, J., W. Melander, G. Vaisnys, and Cs. Horváth, "Kinetic Study on Cis-Trans Proline Isomerization by High-Performance Liquid Chromatography," *J. Phys. Chem.*, **88**, 4536 (1984).

Jaulmes, A., and C. Vidal-Madjar, "Theoretical Aspects of Quantitative Affinity Chromatography: An Overview," *Advances in Chromatography*, Vol. 28, J. C. Giddings, ed., Marcel Dekker, New York, p. 1 (1989).

Jennissen, H. P., "Protein Adsorption Hysteresis," *Proteins at Interfaces: Physiochemical Aspects and Biomedical Studies*, Chap. 9, J. L. Brash and T. A. Horbett, eds., Amer. Chem. Soc., Washington, DC (1987).

Karger, B. L., J. N. LePage, and N. Tanaka, "Secondary Chemical Equilibria in High-Performance Liquid Chromatography," *High Performance Liquid Chromatography*, Vol. 1, Academic Press, New York, p. 113 (1980).

Karger, B. L., and R. Blanco, "The Effect of On-Column Structural Changes of Proteins on their HPLC Behavior," *Talanta*, **36** (1/2), 243 (1989).

Katzenstein, G. E., S. A. Vrona, R. J. Wechsler, B. L. Steadman, R. V. Lewis, and C. R. Middaugh, "Role of Conformational Changes in the Elution of Proteins from Reversed-Phase HPLC Columns," *Proc. Nat. Acad. Sci. U.S.A.*, **83**, 4268 (1986).

Kerlavage, A. R., C. J. Weitzmann, T. Hasan, and B. S. Cooperman, "Reversed-Phase High-Performance Liquid Chromatography of *escherichia coli* Ribosomal Proteins: Characteristics of the Separation of a Complex Protein Mixture," *J. Chromatog.*, **266**, 225 (1983).

Keller, R. A., and J. C. Giddings, "Multiple Zones and Spots in Chromatography," *J. Chromatog.*, **3**, 205 (1960).

Kim, S. U., J. A. Berninger, Q. Yu., and N.-H. L. Wang, "Peak Compression in Stepwise pH Elution with Flow Reversal in Ion Exchange Chromatography," *Ind. Eng. Chem. Res.*, **31**, 1717 (1992).

Klinkenberg, A., "Chromatography of Substances Undergoing Slow Reversible Chemical Reactions," *Chem. Eng. Sci.*, **15**, 255 (1961).

Kunitani, M., D. Johnson, and L. R. Snyder, "Model of Protein Conformation in the Reversed-Phase Separation of Interleukin-2 Muteins," *J. Chromatog.*, **371**, 313 (1986).

Kunitani, M. G., R. L. Cunico, and S. J. Staats, "Reversible Subunit Dissociation of Tumor Necrosis Factor During Hydrophobic Interaction Chromatography," *J. Chromatog.*, **443**, 205 (1988).

Langer, S. H., J. Y. Yurchak, and J. E. Patton, "The Gas Chromatography Column as a Chemical Reactor," *Ind. Engr. Chem.*, **61**(4), 10 (1969).

Lee, C. Y., "Analysis of Adsorption, and Elution Processes in Immobilized Metal Ion Affinity Chromatography," MS Thesis, Purdue Univ., West Lafayette, IN (1991).
Lin, S.-W., and B. L. Karger, "Reversed-Phase Chromatographic Behavior of Proteins in Different Unfolded States," *J. Chromatog.*, **499**, 89 (1990).
Lu, X. M., K. Benedek, and B. L. Karger, "Conformational Effects in the High-Performance Liquid Chromatography of Proteins. Further Studies of the Reversed-Phase Chromatographic Behavior of Ribonuclease A," *J. Chromatog.*, **359**, 19 (1986).
Lu, X.-M., A. Figueroa, and B. L. Karger, "Intrinsic Fluorescence and HPLC Measurement of the Surface Dynamics of Lysozyme Adsorbed on Hydrophobic Silica," *J. Am. Chem. Soc.*, **110**, 1978 (1988).
Mackie, J. S., and P. Meares, "The Diffusion of Electrolytes in a Cation-Exchange Resin Membrane," *Proc. Roy. Soc. London, Ser. A*, **232**, 498 (1955).
Muller, A. J., and P. W. Carr, "Examination of Kinetic Effects in the High-Performance Liquid Affinity Chromatography of Glycoproteins by Stopped-Flow and Pulsed Elution Methods," *J. Chromatog.*, **294**, 235 (1984).
Oroszlan, P., R. Blanco, X.-M. Lu. D. Yarmush, and B. L. Karger, "Intrinsic Fluorescence Studies of the Kinetic Mechanism of Unfolding of α-Lactalbumin on Weakly Hydrophobic Chromatographic Surfaces," *J. Chromatog.*, **500**, 481 (1990).
Parente, E. S., and D. B. Wetlaufer, "Influence of Urea on the High-Performance Cation-Exchange Chromatography of Hen Egg White Lysozyme," *J. Chromatog.*, **288**, 389 (1984a).
Parente, E. S., and D. B. Wetlaufer, "Effects of Urea-Thermal Denaturation on the High-Performance Cation-Exchange Chromatography of α-Chymotrypsinogen-A," *J. Chromatog.*, **314**, 337 (1984b).
Petzold, L. R., "DASSL: A Differential/Algebraic System Solver," Lawrence Livermore National Laboratory, CA (1982).
Regnier, F. E., "High Performance Ion-Exchange Chromatography," *Methods in Enzymology*, Volume 104, *Enzyme Purification and Related Techniques*, W. B. Jakoby, ed., Academic Press, p. 170 (1984).
Regnier, F. E., "The Role of Protein Structure in Chromatographic Behavior," *Sci.*, **238**, 319 (1987).
Schoenmakers, P. J., H. A. H. Billiet, R. Tijssen, and L. De Galan, "Gradient Selection in Reversed-Phase Liquid Chromatography," *J. Chromatog.*, **149**, 519 (1978).
Scopes, R. K., *Protein Purification. Principles and Practice*, Springer-Verlag, New York (1982).
Snyder, L. R. "Gradient Elution," *High-Performance Liquid Chromatography-Advances and Perspectives*, Vol. 1, Chap. 2, Cs. Horváth, ed., Academic Press, p. 207 (1980).
Van Cott, K. E., R. D. Whitley, and N.-H. L. Wang, "Effects of Temperature and Flow Rate on Frontal and Elution Chromatography of Aggregating Systems," *Sep. Technol.*, **1**, 142 (1991).
Velayudhan, A., and M. R. Ladisch, "Role of the Modulator in Gradient Elution Chromatography," *Anal. Chem.*, **63**, 2028 (1991).
Velayudhan, A., and M. R. Ladisch, "Effect of Modulator Sorption in Gradient Elution Chromatography: Gradient Deformation," *Chem. Eng. Sci.*, **47**(1), 233 (1992).
Villermaux, J., "The Chromatographic Reactor," *Percolation Process-Theory and Applications*, A. E. Rodrigues and D. Tonduer, eds., Sijthoff & Noordhoff, Alphen aan den Rijn, The Netherlands, 539 (1981).
Wetlaufer, D. B., and M. R. Koenigbauer, "Surfactant-Mediated Protein Hydrophobic Interaction Chromatography," *J. Chromatog.*, **359**, 55 (1986).
Whitley, R. D., J. M. Brown, N. P. Karajgikar, and N.-H. Linda Wang, "Determination of Ion Exchange Equilibrium Parameters of Amino Acid and Proteins Systems by an Impulse Response Technique," *J. Chromatog.*, **483**, 263 (1989).
Whitley, R. D., K. E. Van Cott, J. A. Berninger, and N.-H. L. Wang, "Effects of Protein Aggregation in Isocratic Nonlinear Chromatography," *AIChE J.*, **37**(4), 555 (1991a).
Whitley, R. D., J. A. Berninger, N. Rouhana, and N.-H. L. Wang, "Nonlinear Gradient Isotherm Parameter Estimation for Proteins with Consideration of Salt Competition and Multiple Forms," *Biotechnol. Prog.*, **7**(6), 544 (1991b).
Whitley, R. D., K. E. Van Cott, and N.-H. L. Wang, "Analysis of Nonequilbrium Adsorption/Desorption Kinetics and Implications for Analytical and Preparative Chromatography," *Ind. Eng. Chem. Res.*, **32**(1), 149 (1993).
Wilson, E. J., and C. J. Geankoplis, "Liquid Mass Transfer at Very Low Reynolds Numbers in Packed Beds," *Ind. Eng. Chem. Fundam.*, **5**(1), 9 (1966).
Wu, S.-L., K. Benedek, and B. L. Karger, "Thermal Behavior of Proteins in High-Performance Hydrophobic-Interaction Chromatography. On-line Spectroscopic and Chromatographic Characterization," *J. Chromatog.*, **359**, 3 (1986a).
Wu, S.-L., A. Figueroa, and B. L. Karger, "Protein Conformational Effects in Hydrophobic Interaction Chromatography. Retention Characterization and the Role of Mobile Phase Additives and Stationary Phase Hydrophobicity," *J. Chromatog.*, **371**, 3 (1986b).
Zhang, X., "Effect of Protein Denaturation in Nonlinear Isocratic and Gradient Elution Chromatography," MS Thesis, Purdue Univ., West Lafayette, IN (1991).

Manuscript received Mar. 31, 1993, and revision received Aug. 31, 1993.